

# (36) RELATIONSHIPS BETWEEN FAILURE BEHAVIOR AND BOLTED CONNECTION STRENGTH OF PULTRUDED GFRP REINFORCED BY MULTIAXIAL GLASS FIBER SHEETS

Phan Viet Nhut<sup>1</sup>, Hideki Takashima<sup>2</sup>, Yukihiro Matsumoto<sup>3</sup>, Yasuo Kitane<sup>4</sup>, and Kunitaro Hashimoto<sup>5</sup>

<sup>1</sup>Member of JSCE, Graduate student, Dept. of Architecture and Civil Engineering, Toyohashi Univ. of Technology (1-1 Hibarigaoka, Tempaku-cho, Toyohashi, Aichi, 441-8580, Japan)  
E-mail: p175510@edu.tut.ac.jp

<sup>2</sup> Member of AIJ, Graduate student, Dept. of Architecture and Civil Engineering, Toyohashi Univ. of Technology (1-1 Hibarigaoka, Tempaku-cho, Toyohashi, Aichi, 441-8580, Japan)  
E-mail: h163527@edu.tut.ac.jp

<sup>3</sup>Member of JSCE, Associate Professor, Dept. of Architecture and Civil Engineering, Toyohashi Univ. of Technology (1-1 Hibarigaoka, Tempaku-cho, Toyohashi, Aichi, 441-8580, Japan)  
E-mail: y-matsum@ace.tut.ac.jp

<sup>4</sup> Member of JSCE, Associate Professor, Dept. of Civil and Earth Resources Engineering, Kyoto Univ. (Kyoto daigaku-katsura, Nishikyo-ku, Kyoto 615-8530, Japan)  
E-mail: kitane.yasuo.2x@kyoto-u.ac.jp

<sup>5</sup> Member of JSCE, Associate Professor, Dept. of Civil Engineering, Kobe Univ. (1-1 Rokkodai-cho, Nada, Kobe, Hyogo, 657-8501, Japan)  
E-mail: hashimoto@person.kobe-u.ac.jp

Pultruded Fiber Reinforced Polymers (PFRP) have been increasingly used in the field of engineering constructions because of their advanced characteristics like lightweight, high strength, and easily molding process. In civil engineering structures, mechanical connections such as bolted connection are widely used because it is an easy way to connect the members. However, this kind of connection for PFRP has low shear strength, reducing the mechanical performance of the connections. In order to overcome this problem, thin multiaxial glass fiber sheets (GF) molded by VaRTM methods can be effectively used to strengthen the PFRP connections. In this paper, two types of GF sheets (0/90 degrees and  $\pm 45$  degrees) were used to strengthen the connections. The strengthening effects of GF sheets for the connections and failure modes of connections will be investigated by tensile shear tests. Then, the relationship between failure modes of the connections and bolted connection strength, including bearing strength and shear-out strength will be investigated. Moreover, this study was conducted for the purpose of examining the formulas of the evaluation of PFRP-bolted connection strength reinforced by multiaxial GF sheets.

**Key Words:** FRP, bearing strength, shear-out strength, failure modes

## 1. INTRODUCTION

Pultruded fibre reinforced polymer (PFRP) structures have been increasingly used in civil infrastructure applications due to advanced properties such as high specific strength, low weight, high corrosion resistance, and fatigue-resisting capacity. In civil engineering structures, mechanical connections such as bolted connection are used widely because it is an easy way to connect the members. However, the major challenge with this kind of connection is that severe stress concentration occurs at the bolt holes,

which reduces the performance of the structures<sup>1)</sup>. Moreover, PFRPs lack connection strength because of its low shear strength. This usually leads the shear-out failure when the ratios between end distance to hole diameter are small ( $e/\phi$ ). This mode of failure is mainly caused by shear stresses and occurs along shear-out planes on the hole boundary in the principal fastener load direction. Thin multiaxial glass fiber sheets also have many advanced characteristics such as high strength, lightweight, and are easy for molding with any shapes. However, multiaxial FRPs lack

elastic modulus and large-scale production performance. Thin multiaxial glass fiber sheets can be combined with epoxy to create thin sheets that can be used for strengthening of PFRP connection. The advanced properties of two kinds of materials can be combined together to create reasonable FRP connections in the field of civil engineering. In this study, we will use the vacuum assisted resin transfer molding (VaRTM) method to create GF sheets and use these sheets to strengthen the performance of the connections.

The design of bolted connections with GF sheets strengthening is much more complex than other standard materials such as steel. The GF sheets can increase the connection strength of PFRP members<sup>2)</sup>. The failure modes of PFRP specimens when strengthened with different GF sheets are different as well depending on the types of GF sheets. As a result, the strengthening effects of different types of GF sheets need to be investigated to develop this strengthening application. In this paper, the strengthening effects of different types of GF sheets for the PFRP connections will be investigated. Then, a series of experiments to determine the fundamental connection strength including bearing strength and shear-out strengths of different types of GF sheets and PFRP members. These fundamental strengths will be used to explain for the relationships between failure modes and connection strengths of FRP connection reinforced by GF sheets. Finally, the formulas for evaluating the strength of PFRP strengthened by GF sheets were proposed according to the failure modes of the connections.

## 2. ULTIMATE STRENGTH OF BOLTED CONNECTIONS

The ultimate strength of bolted connections can be calculated depending on the types of failure modes. Fig.1 shows the different types of failure modes of bolted connections.

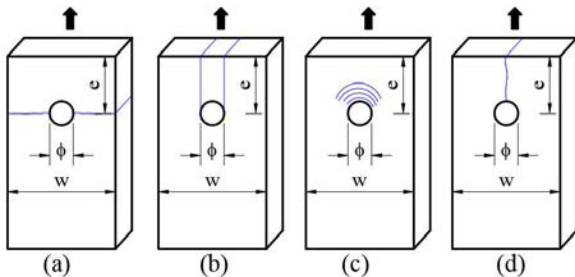


Fig.1 Basic failure modes for bolted connections: (a) net tension, (b) shear-out, (c) bearing, and (d) cleavage.

When members are subjected to a tensile load and failure mode is net tension as shown in Fig.1a, the

average net stress  $\sigma_n$  across a section is calculated from equation (1).

$$\sigma_n = \frac{P}{(w - n\phi)t} \quad (1)$$

where  $P$  is the ultimate tensile load at the joint having a width  $w$  and thickness  $t$ . The number of bolts within the section is  $n$  having a diameter  $\phi$ .

If the failure mode is shear-out failure as shown in Fig.1b, the shear stress  $\tau$  in a joint is calculated by the following equation.

$$\tau = \frac{P}{2et} \quad (2)$$

where  $P$  is the applied load with thickness  $t$  and a distance from the bolt hole center to the ends of the connected plates is  $e$ .

When the failure modes of connection are bearing or cleavage as shown in Fig.1c and Fig.1d, the average bearing stress at the cross-section of the hole can be calculated by equation (3).

$$F = \frac{P}{nt\phi} \quad (3)$$

where  $P$  is the load applied,  $n$  is the number of bolts with the diameter  $\phi$  and with a material thickness of  $t$ . Bearing stress is caused by compression of half the bolt hole transferred by the bolt.

## 3. THE STRENGTHENING EFFECTS OF GF SHEETS FOR PFRP CONNECTIONS

### (1) Materials used for test specimens

#### a) PFRP Channels

In this study, the adopted PFRP consisted of chopped strand mats (CSM), glass roving (UD), and unsaturated polyester resin. The original plates had the C sectional shape as shown in Fig.2. The main parts of the plates were cut to be used in the experiments.

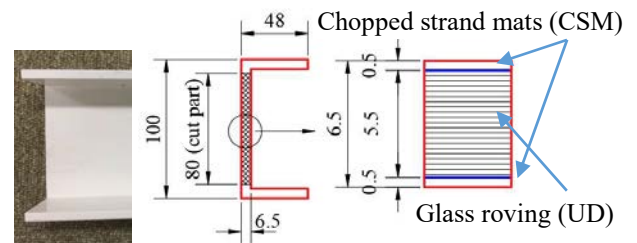


Fig.2 PFRP channel

#### b) Multiaxial glass fiber sheets (GF sheets)

Two types of GF sheets (0/90 degrees and  $\pm 45$  degrees) were used to strengthen the PFRP connections. GF sheets were molded from vacuum-assisted resin transfer molding (VaRTM) method.

Fig.3 shows the diagram of the strengthening

method. The GF sheets were bonded to the PFRP surfaces by E250 resin. In this figure,  $t_{CSM}$  is the thickness of chopped strand mats,  $t_{UD}$  is thickness of glass roving,  $t_{GF}$  is the thickness of GF sheets, and  $T$  is the total thickness of the connections.

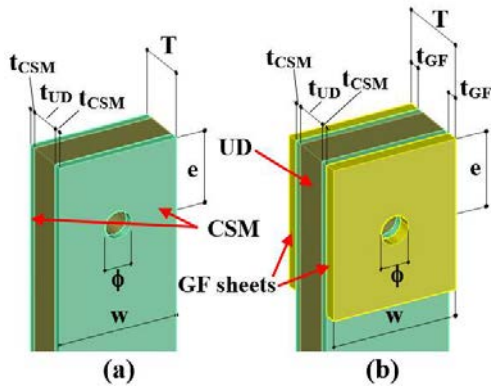


**Fig.3** Strengthening diagram of GF sheets for PFRP connections: (a) PFRP and (b) PFRP with strengthened GF sheets

### c) Experimental programme

**Fig.4** shows the specimen configuration and test setup for tensile experiments. In the experiments, the diameters of the bolt holes ( $\phi$ ) were 16mm for all the cases. The total length of specimens was denoted by  $h$ . **Table 1** shows all the specimens for the tensile tests. There were 9 specimens in total with 3 specimens in every type. In the table, W/o means the specimens without GF sheet strengthening, 0/90 means specimens that were strengthened by 0/90 degrees GF sheets, and  $\pm 45$  means the specimens that were strengthened by  $\pm 45$  degrees GF sheets. The GF sheets were bonded on the surfaces of PFRP after molding by VaRTM method. Then, drilling holes were conducted after curing of the bonding.

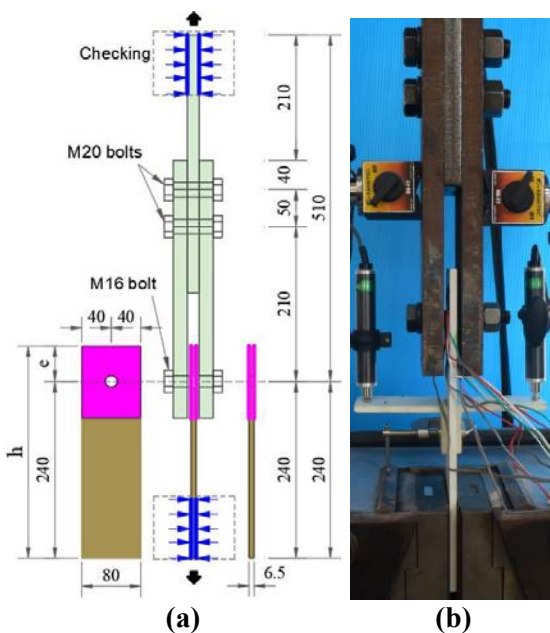


**Fig.4** (a) Specimen configuration and (b) test setup

**Table 1.** All specimens for tensile tests

Specimen	$e$ mm	$T$ mm	$t_{UD}$ mm	$t_{CSM}$ mm	$t_{GF}$ mm
W/o-1	48	6.5	5.5	1	0
W/o-2	48	6.5	5.5	1	0
W/o-3	48	6.5	5.5	1	0
0/90-1	48	7.7	5.5	1	1.2
0/90-2	48	7.7	5.5	1	1.2
0/90-3	48	7.7	5.5	1	1.2
$\pm 45$ -1	48	7.7	5.5	1	1.2
$\pm 45$ -2	48	7.7	5.5	1	1.2
$\pm 45$ -3	48	7.7	5.5	1	1.2

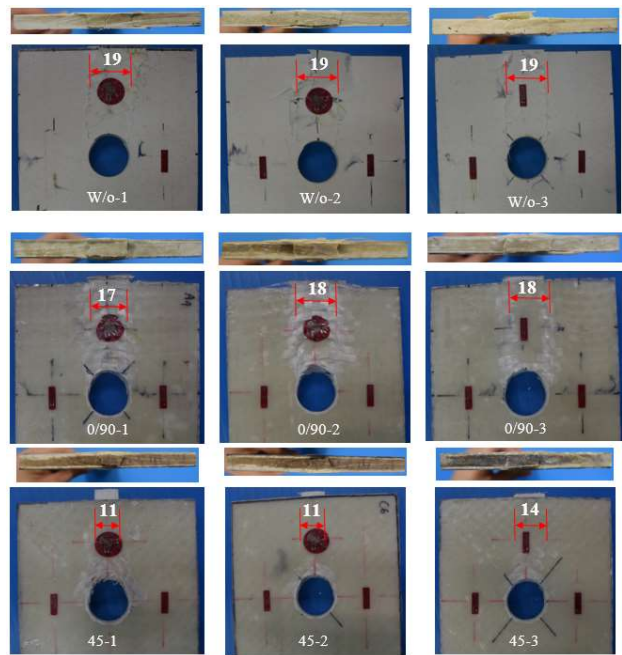


**Fig.5** Failure modes of all specimens

**Fig.5** shows the deformation modes of all specimens. It can be seen from the figure that shear-out failures occurred in all specimens without strengthening. When strengthened with GF sheets, the failure modes of the connection were different. Shear-out failures occurred in the specimens with 0/90 degrees GF strengthening sheets on the whole width of specimens. On the other hand, when strengthening with  $\pm 45$  degrees GF sheets, shear-out failure occurred on the glass roving parts and bearing failures occurred on the chopped strand mats parts and GF sheets.

**Fig.6** shows the load-displacement relations of all specimens. **Table 2** shows the maximum loads obtained from the experiments and strengthening effects of GF sheets on the increase of connection strengths. It is clear that the connections got the highest strengthening effects when strengthened with  $\pm 45$  degrees GF sheets, around 74%; whereas, the strengthening effect was around 49% when using

0/90 degrees GF strengthening sheets.

**Table 2.** Maximum loads of all specimens

Specimen	W/o	0/90	±45
Load (kN)	13.05	17.58	21.54
Average load (kN)	10.78	17.85	20.00
Strengthening effects (%)	---	48.55	73.97

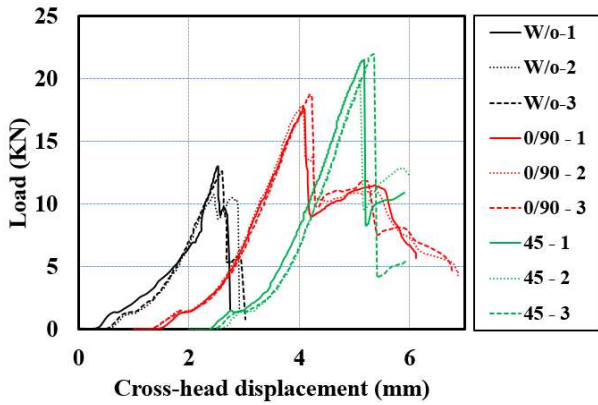


**Fig.6** Load-displacement relations of specimens

#### 4. RELATIONSHIPS BETWEEN FAILURE MODES AND STRENGTH OF PFRP CONNECTION

In section 3, the strengths of PFRP connection increased when strengthened with GF sheets and the failure modes of specimens changed depending on the types of strengthened-GF sheets. Therefore, the relationships between connection strength and failure modes need to be investigated clearly. In this section, we propose equations to calculate the connection strength of PFRP and GF strengthened – PFRP specimens and compare with the experimental results.

The different failure modes of the connection can be found in **Fig.7**. The shear-out failures that were seen in W/o and 0/90 specimens were explained by **Fig.7a** when the shear-out failures occurred in the whole thickness of specimens. **Fig.7b** shows the failure modes when only bearing failures occurred in the whole thickness of the specimens. There is a mixed failure mode as shown in **Fig.7c** where shear-out failure occurred in the glass roving parts and bearing failures occurred in the CSM and GF sheets. The failure modes of specimens ±45 were same with **Fig.7c**. In the figure,  $b$  denotes for the width of shear-out parts.

From the failure modes, we propose the equations to calculate the ultimate tensile loads for the connection as below.

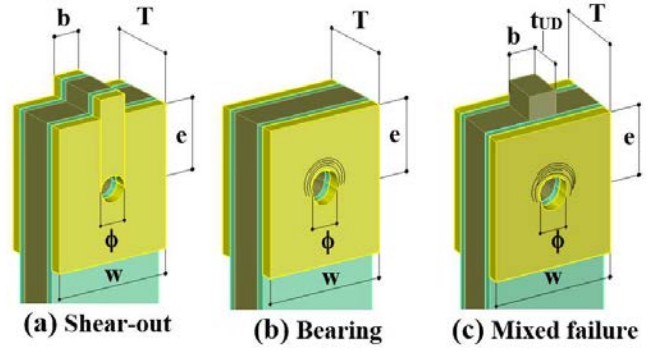


**Fig.7** Failure modes of PFRP connections

$$P_1 = 2 \cdot e \cdot (t_{UD} \cdot \tau_{UD} + t_{GF} \cdot \tau_{GF} + t_{CSM} \cdot \tau_{CSM}) \quad (4)$$

$$P_2 = \phi (t_{UD} \cdot F_{UD} + t_{GF} \cdot F_{GF} + t_{CSM} \cdot F_{CSM}) \quad (5)$$

$$P_3 = 2 \cdot e \cdot (b + t_{UD}) \cdot \tau_{UD} + \phi (t_{GF} \cdot F_{GF} + t_{CSM} \cdot F_{CSM}) \quad (6)$$

The equations (4), (5), and (6) used to calculate the ultimate tensile loads for the connections that have the failure modes as shown in **Fig.7a**, **7b**, and **7c** respectively. Here  $\tau_{GF}$ ,  $\tau_{UD}$ , and  $\tau_{CSM}$  are the shear stress of GF sheets, glass roving, and chopped strand mats respectively.  $F_{GF}$ ,  $F_{UD}$ , and  $F_{CSM}$  are the bearing stress of GF sheets, glass roving, and chopped strand mats respectively.

#### 5. BEARING AND SHEAR STRENGTH OF COMPONENTS OF THE CONNECTIONS

In this section, the bearing strength and shear strength of every component of the connections (chopped strand mats, glass roving, and GF sheets) were investigated by a series of experiments. These values are necessary to consider the validity of the proposed equations in order to calculate the connection strength of PFRP.

##### (1) Bearing tests for components

###### a) Bearing tests for glass roving

As mentioned in section 3, the PFRP channels have two parts: glass roving at the center section with the thickness around 5.5mm and chopped strand mats at the outside with the total thickness around 1mm. In this experiment, the chopped strand mats parts were removed by sanding and glass roving will be used for bearing tests. There were 4 specimens in total with the name from BR1 to BR4 and dimensions  $w \times h = 80 \times 288$  mm. The tensile tests were conducted with the same process of the main tests in section 3. The values of  $3\phi$  were chosen for distances  $e$  in all specimens and the diameters of the holes  $\phi$  are equal to 16mm.

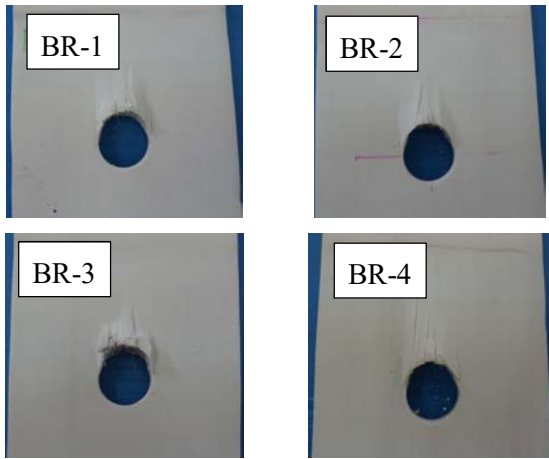


Fig.8 Failure modes of bearing tests for UD

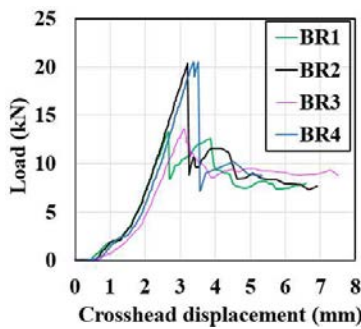


Fig.9 Load-displacement relations of bearing tests of UD

Table 3. Ultimate bearing stress of UD

Specimen	1	2	3	4	Average
$P_{UD}$ (kN)	13.28	20.38	13.62	20.56	---
Thickness (mm)	4.91	4.89	4.79	4.92	---
$F_{UD}$ (MPa)	168.97	260.63	177.69	261.20	217.12

Tensile tests were performed in the same processes in section 3. Fig.8 shows the failure modes of glass roving under bearing tests. Fig.9 shows maximum loads and relations between loads and displacements obtained from experiments. The average values of bearing strengths of glass roving were calculated as shown in Table 3. In this table,  $P_{UD}$  means the ultimate bearing loads for UD specimens. The ultimate bearing stress was calculated from equation (3).

#### b) Bearing tests for chopped strand mats

In order to investigate the bearing stress of chopped strand mats, we used the same types of CSM in PFRP members to mold the CSM plates using VaRTM method. The molding process and tensile tests were the same in section 3. Then, total 3 specimens of CSM plates (BCSM1 to BCSM3) were cut with the dimensions  $w \times h = 80 \times 288$  mm. After cutting, the CSM plates were drilled the holes. The same values of  $e$  ( $3\phi$ ) and  $\phi$  (16mm) were chosen in all

specimens.

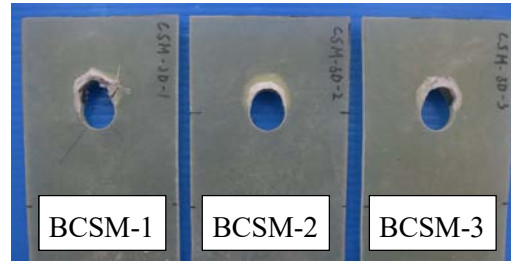


Fig.10 Failure modes of CSM bearing specimens

Fig.10 shows the bearing failures of CSM plates. Fig.11 shows maximum loads and relations between loads and displacements obtained from experiments. The average values of bearing strengths of CSM were calculated as shown in Table 4. In this table,  $P_{CSM}$  means the ultimate bearing loads for CSM specimens. The ultimate bearing stress was calculated from equation (3).

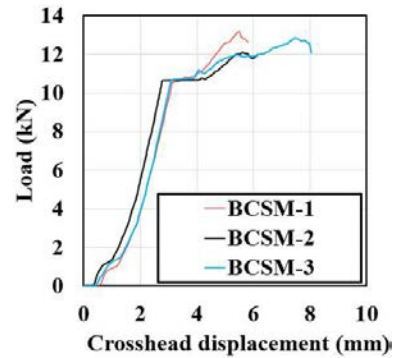


Fig.11 Load-displacement relations of bearing tests of CSM

Table 4. Ultimate bearing stress of UD

Specimen	2	3	4	Average
$P_{CSM}$ (kN)	13.16	12.11	11.18	---
Thickness (mm)	4.60	4.80	4.70	---
$F_{CSM}$ (MPa)	178.75	157.65	148.69	161.69

#### c) Bearing tests for GF sheets

The same processes of molding and tensile tests with bearing tests of CSM plates were conducted with GF sheets to determine the bearing strength of GF sheets.

Two types of GF plates were molded including 0/90 degrees and  $\pm 45$  degrees GF plates. Total 4 specimens for every type of GF plate (B0/90-1 to B0/90-4 and B45-1 to B45-4) were prepared for the bearing tests. All the specimens have the dimensions  $w \times h = 80 \times 288$  mm. The values of 48mm ( $3\phi$ ) for  $e$  and 16mm ( $\phi$ ) were also chosen to drill the bolt holes.

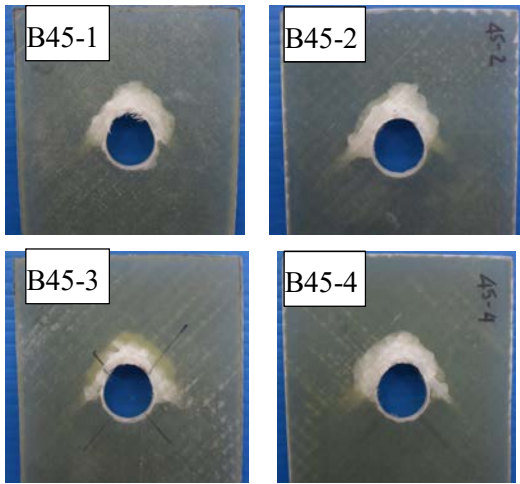


Fig.12 Bearing failures of  $\pm 45$  degrees GF plates

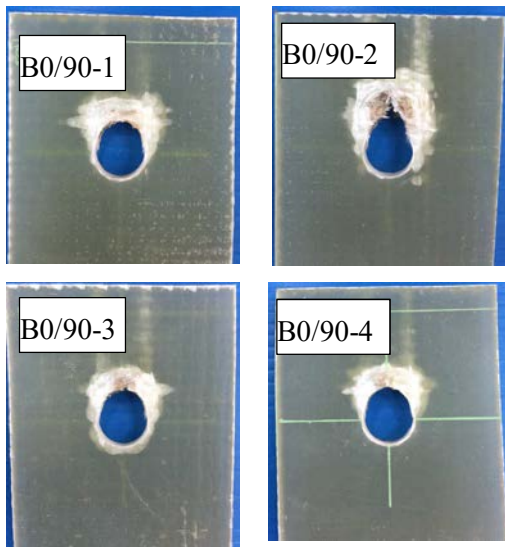


Fig.13 Bearing failures of 0/90 degrees GF plates

Fig.12 and Fig.13 show the bearing failures of  $\pm 45$  degrees and 0/90 degrees GF plates, respectively. Fig.14 and Fig.15 show the load-displacement relations of  $\pm 45$  degrees and 0/90 degrees GF plates, respectively. The ultimate bearing stresses of GF plates were calculated from equation (3) and the results are shown in Table 5.

Table 5. Ultimate bearing stress of GF plates

Specimen	1	2	3	4	Average
$P_{45}$ (kN)	14.42	13.84	11.49	12.07	---
Thickness (mm)	6.10	5.56	5.61	5.67	---
$F_{45}$ (MPa)	147.69	155.60	128.06	133.03	141.10
$P_{0/90}$ (kN)	10.67	11.98	10.80	9.87	---
Thickness (mm)	5.46	5.61	5.49	5.46	---
$F_{0/90}$ (MPa)	122.18	133.42	123.00	112.99	122.90

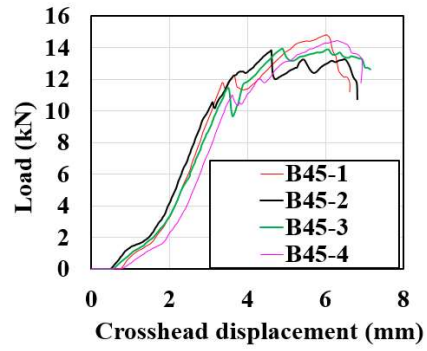


Fig.14 Load-displacement relations of bearing tests of  $\pm 45$  degrees GF plates

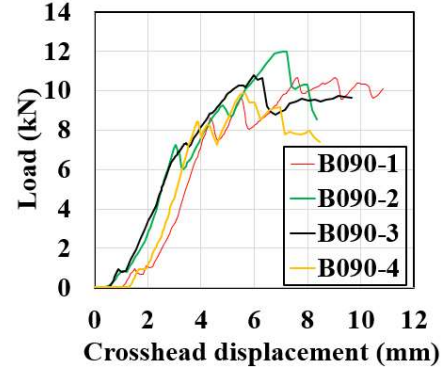


Fig.15 Load-displacement relations of bearing tests of  $\pm 45$  degrees GF plates

## 2) Shear tests for components

### a) Shear test for glass roving

In this test, the chopped strand mats from PFRP channel were removed and glass roving parts were used for shear-out tests with tensile loads. Total 2 specimens with the dimensions  $w \times h = 80 \times 288$  mm were used for the tests. The distance  $e$  is 48mm ( $3\phi$ ) and the diameter of the bolt hole ( $\phi$ ) is 16mm. Fig.16 shows the shear-out failures of UD plates. The ultimate shear-out stresses of the connections were calculated from equation (2). Fig.17 shows the load-displacement relations of the shear-out tests for UD. Table 6 shows the calculated results.

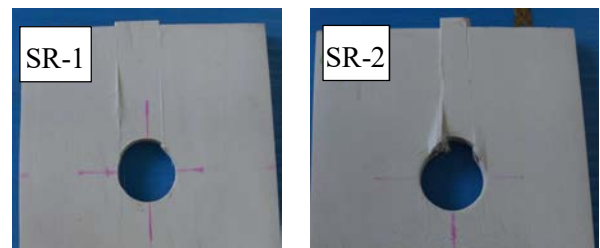
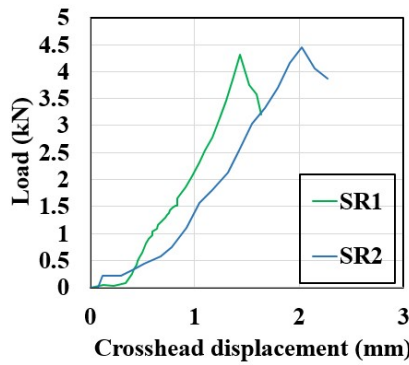


Fig.16 Shear-out failures of glass roving plates

### b) Shear test for GF sheets and CSM

Because the shear stress of GF sheets and CSM are higher than UD, the shear-out investigations are difficult by normal tensile tests. In this part, the shear

stresses of GF sheets and CSM will be determined by V-Notched Rail Shear Method<sup>3)</sup> (according to Standard ASTM D7078). **Fig.18** shows the V-Notched Rail Shear machine and test setup for shear tests. This test method covers the determination of the shear properties of high-modulus fiber-reinforced composite materials by clamping the ends of a V-notched specimen between two pairs of loading rails. When loaded in tension, the rails introduce shear forces into the specimen through the specimen faces.



**Fig.17** Load-displacement relations of shear tests of UD

**Table 6.** Ultimate shear-out stress of UD plates

Specimen	1	2	Average
$P_{UD}$ (kN)	4.31	4.44	
Thickness (mm)	4.84	4.87	
$\tau_{UD}$ (MPa)	9.27	9.50	9.39

The specimens in V-Notched shear test have dimensions of 56×76mm. All the specimens of GF sheets and CSM were molded by VaRTM method. Then, a total of 5 specimens of GF sheet ( $\pm 45$  and 0/90 degrees) and 4 specimens of CSM sheets were cut. These specimens were named as S45-1 to S45-5 for  $\pm 45$  degrees GF sheets, S0/90-1 to S0/90-5 for 0/90 degrees GF sheets, and SCSM-1 to SCSM-4 for CSM sheets.

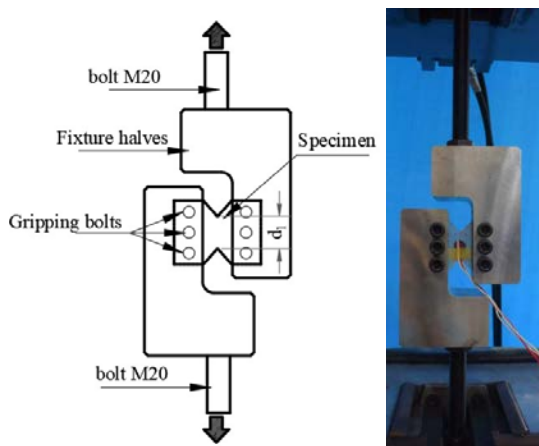


**Fig.18** V-notched Rail Shear Apparatus and test setup

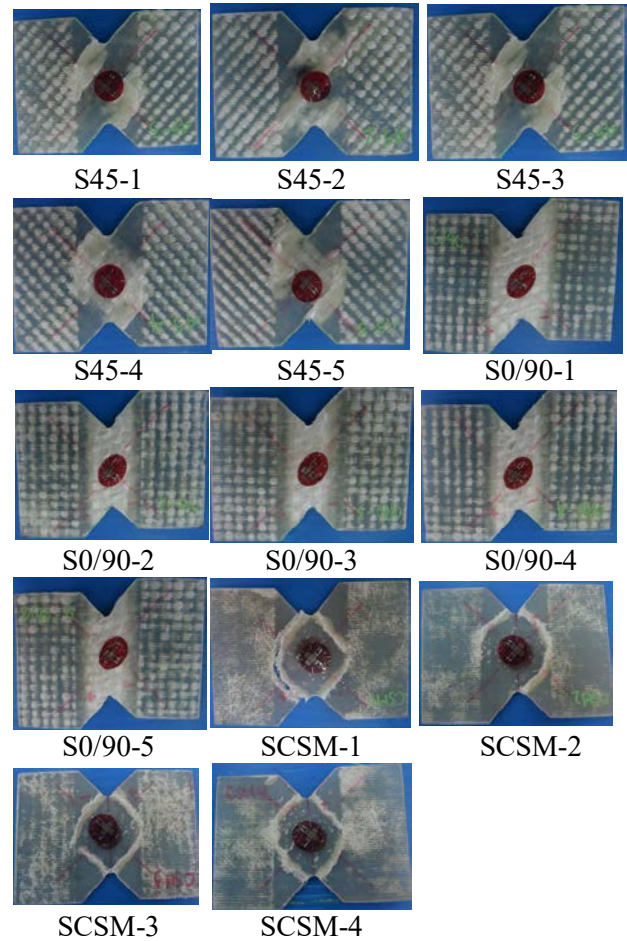


**Fig.19** Shear failures of specimens

Shear stress of specimen with the thickness  $t$  is calculated by equation (7)

$$\tau = \frac{P}{A} = \frac{P}{t \cdot d_1} \quad (7)$$

where  $P$  is the shear load in the experiments.

**Fig.19** shows the failure modes of  $\pm 45$  degrees GF sheets, 0/90 degrees GF sheets, and CSM sheets. The shear failures at the center section of specimens can be seen clearly in specimens S0/90. On the other hand, shear failures occurred in the direction  $\pm 45$  degrees in specimens S45; whereas, a combined shear failure occurred in SCSM specimens. This is because CSM has multi-axial directional fibers.

**Fig.20, 21, and 22** show the load and displacement relations of all shear specimens. It can be seen from these figures that ultimate shear stress can be determined clearly in  $\pm 45$  degrees GF sheets and CSM sheets. However, ultimate shear stress cannot be determined clearly in 0/90 degrees GF sheets. After initial shear failures occurred, the loads kept increasing gradually because the constraints of 0 degrees fibers. In 0/90 degrees GF sheets, initial shear stress can be investigated at the first peak values of loads. **Table 7** shows the shear stress of all

specimens. In this table, ultimate shear stresses were considered for  $\pm 45$  degrees GF sheets and CSM sheets, while initial shear stresses were calculated for 0/90 degrees GF sheets.

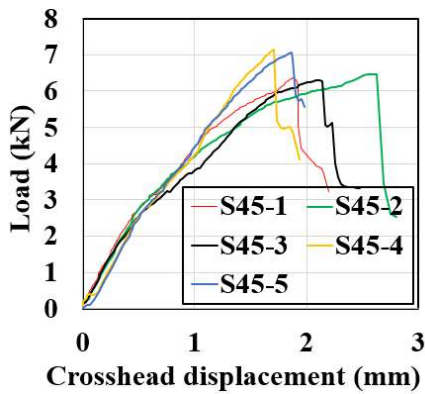


Fig.20 Load-displacement relations of shear tests of  $\pm 45$  degrees GF sheets

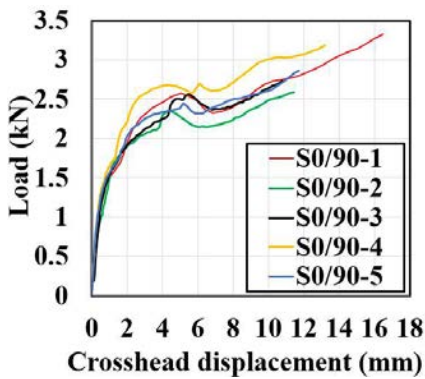


Fig.21 Load-displacement relations of shear tests of 0/90 degrees GF sheets

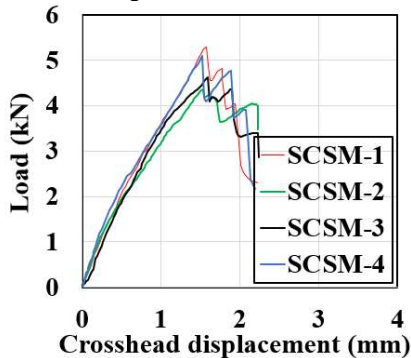


Fig.22 Load-displacement relations of shear tests of CSM sheets

The ultimate shear stress of 0/90 degrees GF sheets cannot be investigated in the V-Notched shear tests. Therefore, another type of experiment will be introduced in the next sub-section to investigate the ultimate shear stresses of 0/90 degrees GF sheets.

Table 7. Ultimate shear stress of  $\pm 45$  GF sheets, CSM sheets and initial shear stress of 0/90 GF sheets

Specimen	1	2	3	4	5	Average
$P_{CSM}$ (kN)	5.30	4.35	4.62	5.09	---	---
$d_1$ (mm)	31.87	31.93	31.55	31.74	---	---
Thickness $t$ (mm)	1.93	1.91	1.93	1.96	---	---
$\tau_{CSM}$ (MPa)	85.94	71.49	75.91	81.69	---	78.76
$P_{45}$ (kN)	6.36	6.47	6.31	7.15	7.08	---
$d_1$ (mm)	31.66	31.95	31.86	31.89	31.50	---
Thickness $t$ (mm)	2.36	2.38	2.36	2.36	2.41	---
$\tau_{45}$ (MPa)	85.04	85.02	83.93	94.91	93.21	88.42
$P_{0/90}$ (kN)	2.58	2.35	2.56	2.68	2.45	---
$d_1$ (mm)	31.51	31.86	31.93	31.52	31.76	---
Thickness $t$ (mm)	2.37	2.40	2.41	2.42	2.42	---
$\tau_{0/90}$ (MPa)	34.52	30.69	33.26	35.20	31.90	33.11

### c) Tensile shear test for 0/90 degrees GF sheets

In this part, tensile tests will be conducted to determine the ultimate shear stress of 0/90 degrees GF sheets. By decreasing the distance  $e$ , the ultimate shear-out stress of 0/90 degrees can be investigated by tensile tests. In this test, the 0/90 degrees GF sheets were molded by VaRTM method with the same process in section 3 and then total 4 specimens (US0/90-1 to US0/90-4) with the dimensions  $w \times h = 80 \times 288$  mm were cut to use for the tests. The distances from the centers of the holes to the edges were set to 24mm ( $1.5\phi$ ) and the values of diameters of the holes were 16mm ( $\phi$ ).

Fig.23 shows the shear failure modes of 0/90 degrees GF sheets. Fig.24 shows the load-displacement relations of all 0/90 degrees GF sheets. Table 8 shows the ultimate shear stress of 0/90 degrees GF sheets. The ultimate shear stresses of specimens were calculated from equation (2).

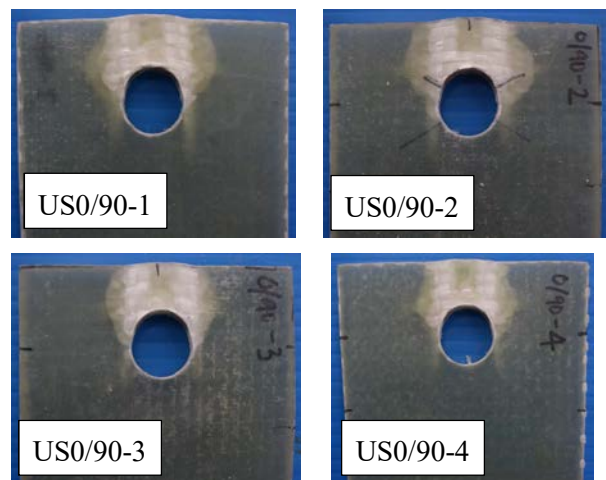


Fig.23 Shear failures of 0/90 degrees GF sheets

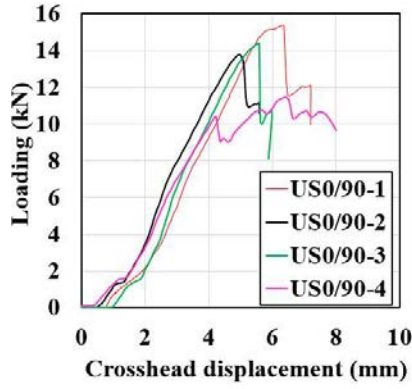


Fig.24 Load-displacement relations of shear-out tests of 0/90 degrees GF sheets

Table 8. Ultimate shear stress of 0/90 GF sheets

Specimen	1	2	3	4	Average
$P_{0/90}$ (kN)	15.39	13.77	14.39	11.45	---
Thickness $t$ (mm)	6.20	5.85	5.90	5.25	---
$\tau_{0/90}$ (MPa)	51.70	49.02	50.82	45.42	49.24

Table 9. Ultimate shear stress and bearing stress of components

Type	UD	0/90GF	$\pm 45$ GF	CSM
Shear-out stress (MPa)	9.39	49.24	88.42	78.76
Bearing stress (MPa)	217.12	122.90	141.10	161.69

#### d) Summary of the stress of components of the connections

Table 9 and Fig.25 show the ultimate shear-out stresses and bearing stresses of UD, CSM, and GF sheets for the connections. The shear-out strength of glass roving is very small compared with other strengths. Therefore, shear-out failures of glass roving occurred in all case without and with GF sheet

strengthening. Bearing stresses got the highest values in CSM and shear-out stresses obtained the highest values in  $\pm 45$  degrees GF sheets.

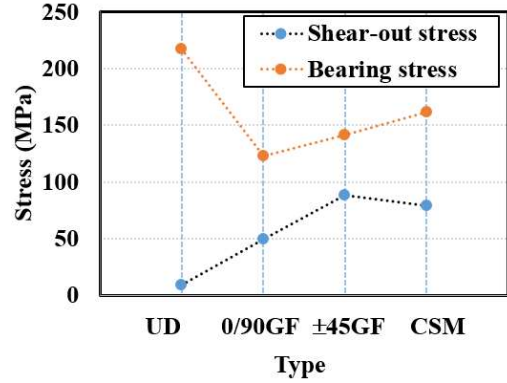


Fig.25 Ultimate stress of components of the connections

## 6. EVALUATION OF STRENGTH OF GF STRENGTHENED – PFRP CONNECTION

In this section, the ultimate tensile loads of PFRP and PFRP reinforced by GF sheets in section 3 will be evaluated according to proposed equations (4), (5), and (6). The connection strengths will be calculated depending on the failure modes of the connections as shown in Fig.7. Table 10 shows the calculated ultimate tensile loads for all specimens. In the table,  $P_e$  is the average values of ultimate tensile loads from experiments and  $P_{eq}$  is the ultimate tensile loads calculated from proposed equations. The ultimate loads obtained from experiments and equations will be compared together to check the accuracy of the equations. The ultimate tensile loads  $P_1$ ,  $P_2$ , and  $P_3$  in Table 10 are corresponding to three kinds of failure modes: shear-out, bearing, and mixed failures respectively, as shown in equation (4), (5), (6), and Fig.7.

Table 10. Ultimate tensile loads of the connections with the comparisons of experimental and proposed equations' results

Specimen	$b$ mm	$\tau_{UD}$ MPa	$\tau_{CSM}$ MPa	$\tau_{GF}$ MPa	$F_{UD}$ MPa	$F_{CSM}$ MPa	$F_{GF}$ MPa	$P_1$ kN	$P_2$ kN	$P_3$ kN	$P_{eq}$ kN	$P_e$ kN	Variation
W/o-1	19	9.39	78.76	0	217.12	161.69	0	12.5	21.69	24.67			
W/o-2	19	9.39	78.76	0	217.12	161.69	0	12.5	21.69	24.67	12.52	12.16	2.95%
W/o-3	19	9.39	78.76	0	217.12	161.69	0	12.5	21.69	24.67			
0/90-1	17	9.39	78.76	49.24	217.12	161.69	122.9	18.2	24.05	25.23			
0/90-2	18	9.39	78.76	49.24	217.12	161.69	122.9	18.2	24.05	26.13	18.19	18.06	0.71%
0/90-3	18	9.39	78.76	49.24	217.12	161.69	122.9	18.2	24.05	26.13			
$\pm 45$ -1	11	9.39	78.76	88.42	217.12	161.69	141.10	22.7	24.40	20.17			
$\pm 45$ -2	11	9.39	78.76	88.42	217.12	161.69	141.10	22.7	24.40	20.17	21.07	21.15	-0.39%
$\pm 45$ -3	14	9.39	78.76	88.42	217.12	161.69	141.10	22.7	24.40	22.87			

As can be seen from the failure modes of specimens after experiments as shown in **Fig.4**, the failure modes of specimen W/o and 0/90 are shear-out failures in the whole thickness of specimens. On the other hand, the failure modes of  $\pm 45$  specimens are mixed failures. Therefore, the ultimate tensile loads of specimen W/o and 0/90 will be determined following to equation (4) and ultimate tensile loads of  $\pm 45$  specimens will be calculated according to equation (6).

There were good correspondences about the values of ultimate tensile loads calculated from proposed equations and experimental results. Therefore, the proposed equations can be used accurately to determine the ultimate tensile loads for the connections of PFRP and GF strengthened – PFRP members.

## 7. CONCLUSIONS

This paper investigated the strengthening effects of thin multiaxial glass fiber sheets for the PFRP connections. The GF sheets can increase the connection strengths of PFRP members effectively, up to 49%

for 0/90 degrees GF sheets and 74% for  $\pm 45$  degrees GF sheets. In addition, the relationships between failure modes and ultimate strengths of the connections were perfectly explained by the proposed equations. Finally, these proposed equations can be used to calculate the ultimate tensile loads for the connections of PFRP strengthened by thin multiaxial glass fiber sheets.

## REFERENCES

- 1) Chen, W. F. (1997). *Handbook of structural engineering*
- 2) 高嶋秀樹, Viet Nhut Phan, 松本幸大, 北根安雄, 橋本国太郎: 多軸基材により補強した引抜成形 GFRP 材のボルト接合強度に関する基礎検討, 日本建築学会東海支部研究報告集(CD-ROM), pp.197-200, 2019.2
- 3) D 7078/D 7078M – 05 Standard Test Method for Shear Properties of Composite Materials by V-Notched Rail Shear Method

(Received August 30, 2019)